Experimental characterization of monotonic and cyclic behavior of steel-to-CLT nailed joints strengthened with composite plies

EXPERIMENTAL CHARACTERIZATION OF MONOTONIC AND CYCLIC BEHAVIOR OF STEEL-TO-CLT NAILED JOINTS STRENGHTENED WITH COMPOSITE PLIES

Alessandro Bellini[1,*], Luca Benedetti[1], Luca Pozza[1,2] , Claudio Mazzotti[1,2]

[1] CIRI Buildings and Construction (CIRI-EC),
University of Bologna, Via del Lazzaretto 15/5, 40131, Bologna, Italy

[2] Department of Civil, Chemical, Environmental and Materials Engineering (DICAM),
University of Bologna, Viale Risorgimento 2, 40136, Bologna, Italy

* Corresponding Author

Tel: +39 051 2090553, email: alessandro.bellini5@unibo.it

ABSTRACT

Connections play a key role in timber structures because they are the parts devoted to energy dissipation during an earthquake or, when specific hysteretic devices are introduced, their hyper-resistant design allows for a rigid fastening of those devices, thus assuring an elastic behavior of the structure under seismic loads. A promising technique to improve both the load-bearing capacity and the stiffness of joints with dowel-type fasteners, consists in increasing the embedment strength of the wood-based materials, usually by applying a superficial reinforcing layer to the timber-connection shear plane interface. In this framework, results of an experimental campaign carried out on steel-to-CLT panel nailed joints strengthened with a carbon fiber ply glued to the shear plane interface are presented and discussed in this paper. Two different load configurations (perpendicular and parallel to the grain) and two different loading protocols (monotonic and cyclic) have been considered, analyzing the results in order to evaluate the effectiveness of the reinforcement technique in terms of load-bearing capacity and stiffness, with respect to the reference unreinforced configuration. Finally, the applicability of the current design method is verified together with the proposal of a simplified design procedure.

KEYWORDS: Local strengthening; Steel-to-CLT panel nailed joint; FRP; composite ply; cyclic behavior.

1. INTRODUCTION

Timber structures are very common in both historical and modern buildings nowadays since they have good structural performance and the lightness guaranteed by wood-based materials. In particular, the use of Cross-Laminated Timber (CLT) panels, in comparison with other timber-based

technologies, progressively increased during the last years, thanks to their performance combined with the simplicity and speed of assembly. One of the key issues of this type of structures is the behavior of the connections [1], because they are usually the elements in charge of dissipating the energy introduced in a structure by the earthquake. For this reason, the load-bearing capacity of the joint area of timber members is the primary weak point when considering the overall load-bearing behavior and stiffness of both existing and new timber constructions.

The effectiveness of joints realized connecting members by using dowel-type fasteners such as nails, screws or dowels is generally included in the 40 - 60% range [2], meaning that the structural joint detailing has a crucial importance on the performance of the whole structure.

From the knowledge of the different failure modes of the joints and of their key influencing parameters, targeted changes to the structural design of the connection may improve its capacity and minimize the amount of material locally required for the member cross-section: i.e., by using fasteners made of high-strength and ductile steel or timber of higher density [2].

The connections in CLT structures are usually realized by using nailed brackets [3] which, however, can be subjected to brittle failure if not properly designed, causing a fragile behavior of the whole structure under seismic actions [4]. An alternative method to dissipate energy is to use specific hysteretic devices [5-7], with the requirement that the whole wooden structure has to behave elastically during the earthquake, needing therefore the design of hyper-resistant connections for fastening the hysteretic dampers to the timber elements.

Among the different available connection technologies, dowel-type fasteners are the most common ones with a mechanical behavior which can be described according to the Johansen theory [8]. In more detail, steel-to-timber joints with dowel-type fasteners may show a defined range of failure modes (i.e. embedment failure of timber or bending failure of the fastener and simultaneous embedment failure of the timber), where the key parameters needed for a proper analysis of the mechanisms are the embedment strength of the timber or wood-based material (e.g. CLT) and the

joint geometry (i.e. thickness of the members to be connected, fasteners spacing, end and edge distances of the fasteners).

The use of nails for the connections represents an optimal solution since they are cheap, they don't require the realization of carpentry notches in timber elements and they can be driven into the wood by beating, ensuring the complete absence of gaps and allowing, in this way, to achieve an high performance of the connection, maintaining however a ductile failure mode.

The need of realizing hyper-resistant and stiff connections requires a proper cost-benefit analysis, since the increment of the number of nails is not always compatible with the size of the standard steel plates and often leads to a loss of efficiency of the connection. Moreover, since the connection has also to ensure a limited damaging during operational conditions, an increment of the number of fasteners increases the area subjected to damage and represents another negative aspect to be taken into account.

In this framework, the aim of the present paper is the development of an innovative steel-to-CLT FRP-strengthened connection hyper-resistant and stiffer than the unreinforced ones. In more details, an experimental campaign has been carried out to analyze the monotonic and cyclic behavior of nailed connections when strengthened with composite plies, evaluating the performance of the local strengthening technique proposed with the purpose of improving the load-bearing capacity and the stiffness of the steel-to-CLT panel nailed joints. The innovative technique used is based on the application of a multiaxial carbon fiber fabric to the surface of the CLT using epoxy resin, in order to realize an additional lightweight and efficient composite reinforcement layer useful for obtaining a hyper-resistant connection.

The efficiency of timber-reinforcement is already known in literature and has been widely studied for connections realized using solid timber or glulam, but to date there are no researches and studies on the applicability of this technique to CLT. In particular, bending and shear strengthening of timber beams with externally bonded composite materials are analyzed in several papers [9-13], while only few studies are available concerning possible solutions for the specific problem of

timber structural joints, such as the reinforcement with fully-threaded screws and external steel plates for dowel joints [2] or glass fibers strengthening systems [14].

At the same time, the growing need of maintaining and upgrading existing constructions has aroused great interest in the last decades pushing more and more the research of traditional or innovative low invasive strengthening techniques based on externally bonded retrofitting systems, such as those based on FRP composite materials [15-19]. Another possibility to increase the load-bearing capacity of the joint is to use nail-plate connectors [20,21], with a larger increase of thickness or CLT panel modifications.

Coupling of high-performance carbon fibers and specific adhesives for realizing a light and highly efficient skin reinforcement is the first step to further improve the mechanical behavior of steel-to-CLT nailed joints. This can be realized by gluing a thin reinforcement on wood-based panels in order to reach an embedment strength much greater than that of the timber which has to be reinforced. This approach is also able to offer additional strengthening against stresses perpendicular to the grain in the area of application of the fasteners, reducing sensitivity to splitting [22]. The strengthening system efficiency can be fully exploited when the failure mode of the connector involves only a superficial layer of the CLT panel and, consequently, the composite reinforcement is suitable for small diameter fasteners (nails and screws), while large diameter connectors, with a failure mode involving a deeper material layer, could experience only a limited benefit.

The presented experimental study is based on monotonic and cyclic tests carried out on unreinforced and strengthened CLT specimens with nailed connections; experimental outcomes are presented in terms of peak loads, displacement capacity and, with the adoption of some linearization methods, yielding force, stiffness and ductility. Finally, the current analytical model adopted for the design of unreinforced connections is specified and used to predict the behavior of the reinforced connections. Results from different analytical models are analyzed and discussed, with the purpose of validating a first simplified design procedure.

2. EXPERIMENTAL PROGRAM

This study is aimed at investigating, by means of experimental monotonic and cyclic tests, the effectiveness of an original technique for improving the load bearing capacity and stiffness of steel-to-CLT panel nailed joints, by using a composite ply glued to the CLT nailed surface.

The experimental campaign, consisting in a total number of 80 tests, is summarized in Table 1. In particular, for each group, number of tests, type of connection, load direction with respect to the grain, presence of the strengthening system, test type (monotonic or cyclic) and failure mode are indicated. Specimens are identified by using a simplified sample code, where the first two characters refer to the diameter of nails used for the connections (N4 = 4 mm, N6 = 6 mm), the letter E, if present, identifies the specimens strengthened with carbon fabric and epoxy resin, the following characters indicate the load to grain inclination (0° or 90°) and the type of loading (M = monotonic, C = cyclic). Depending on the nails diameter, the connections have a common geometrical nails configuration: twelve 4×60 Anker nails (A.N.) for N4 and eight 6×60 Anker Nails for N6. The two nail configurations ensure quite similar strength values; moreover, the area of the CLT panel involved in the nailed connection is almost the same for the two configurations even if different spacing between the fasteners have been used according to both codes and connectors technical approval recommendations [23].

2.1. Materials properties and samples characteristics

CLT panels with dimensions 200 × 600 mm^2 made of 5 crosswise laminated board layers with a total thickness of 100 mm (20 mm per layer) were used in the tests. The grade of the single laminated boards was C24 according to [24], whereas the panels were characterized according to [25]. As prescribed by [26], CLT panels were conditioned at (20 ± 2)°C temperature and (65 ± 5)% humidity before performing the tests until a wood relative humidity of 12% was reached. The CLT panel density was evaluated according to EN 384 [27], obtaining an average value of 438 kg/m^3.

S275 grade steel plates 6 mm thick with dimensions of 100 × 450 mm^2 were used for the connections. Twelve (4×60 mm according to [28]) or eight (6×60 mm according to [28]) annular ringed nails were used to fasten the steel plates to the CLT panels. All the nails were positioned respecting the spacing prescribed by [29] and [23], respectively, for steel and timber connections (see Figure 1), adopting a hole diameter (in the steel plates) equal to 4.25 mm or 6.50 mm to reduce the allowance between the plate and the nails. Experimental tests were performed on nails for both diameters (according to EN 409 [30]), obtaining an average yielding moment of 8282.46 N·mm and of 27840.19 N·mm for 4 mm and 6 mm nails, respectively.

The CLT surface was strengthened by using a balanced multiaxial carbon fabric with a density of 400 g/m^2 (100 g/m^2 per direction), characterized by a dry fiber maximum tensile strength of 3000 MPa, an elastic modulus of 240 GPa, a carbon fiber density of 1780 kg/m^3 [31] and an equivalent dry fiber thickness of 0.056 mm. The carbon textile was glued to the samples substrate by using an epoxy resin, characterized by a density of 1400 kg/m^3 [32], after applying an epoxy primer first. No adhesive was used between the carbon ply and the nailed steel plate.

The bond properties of the FRP to the CLT substrate were preliminary verified by means of single-lap shear tests following standard procedures for composite materials, as described in [17,18,33,34]. Tests showed a perfect adhesion between the composite reinforcement and the CLT panel, leading to the tensile failure of the textile outside of the bonded area. The absence of premature debonding or delamination mechanisms for both the load-grain inclinations allowed to reach the full exploitation of the carbon fabric capacity, highlighting the perfect efficiency of the strengthening system in terms of bond capacity.

2.2. Test configuration and set-up

The experimental set-up adopted for the tests on the connections, which was validated during several experimental campaign performed on FRP composites applied on masonry substrate [17,18], is shown in Figure 2. Samples were placed on a rigid steel frame equipped with front and rear steel reaction elements suitable for preventing horizontal and vertical displacements of the CLT

specimens. The free end of the steel plate (i.e. the part of the plate not connected to the CLT panel) was clamped with five 12 mm 8.8 grade bolts within a two steel plates system and connected to an electromechanical actuator using a central hinge allowing for rotations around the vertical axis. The slip between the steel plate and the actuator was avoided by friction tightening of the bolts.

A class 0.5 load cell with a maximum capacity of 100 kN was used to measure the force applied by the actuator, whereas two 50 mm displacement transducers (LVDTs) were used to measure the relative displacement (slip) between the nailed steel plate and the CLT panel (see Figure 2a and 2b). In particular, LVDTs were fixed on the CLT panel, by means of plastic holders, with the mobile stroke, reading the relative displacement of an L-shaped profile, fixed on the steel plate and located at a distance of 15 mm from the beginning of the nailed part of the connection. Data were recorded during monotonic and cyclic tests adopting a sample rate of 5 Hz.

2.3. Loading protocol

The load protocols adopted during the experimental campaign are shown in Figure 3. The protocol prescribed by EN 26891 [35] was adopted for monotonic tests (Figure 3a). In more detail, tests were carried out under displacement control, imposing a rate of 2 mm/min during the first cycle, performed up to 40% of the maximum estimated capacity, after which load was maintained constant for 30 s and then decreased to 10% of the maximum estimated force; finally, after additional 30 s, displacement was monotonically increased at a rate of 4 mm/min until system failure.

Cyclic tests were carried out according to UNI EN 12512 [36], performing a single cycle repetition up to 25% and 50% of the estimated yield displacement of the connection and three cycles repetitions at, respectively, 75%, 100%, and 200% of this value (see Figure 3b). Tests were performed under displacement control, adopting a test rate of 2 mm/min during the cycles then increased to a maximum value of 4 mm/min during the final loading phase (up to failure of the connection). While all the above described cycles were possible for connections based on 6 mm Anker nails, preliminary tests showed that the reaching of the yielding stress for reinforced and

unreinforced 4 mm Anker nails caused a premature failure of the connection, thus preventing to perform additional cycles after 100% of the connection yield displacement.

3. EXPERIMENTAL RESULTS

Results of monotonic and cyclic tests are presented and discussed in this section in terms of failure modes and force - slip curves.

3.1. Observed failure modes

The failure modes identified during the tests are reported in Table 1 for each group of samples. Three different mechanisms, labeled with the letters A-C, were observed. Figure 4 shows a detailed view of the three mechanisms and, in more detail: Figure 4a refers to an example of embedment failure of the timber panel (i.e. typical failure mode of wood fiber substrate associated to the bending deformation of the nails – type A), Figure 4b refers to a reduced embedment due to the applied composite reinforcement (type B), while Figure 4c shows the embedment of the CLT panel associated to a remarkable surface damage (i.e. wood fiber removal – type C).

Failure mode A (see Figure 4a) is typical of unreinforced specimens loaded parallel to grain independently of the nail diameter, whereas mode C (Figure 4c) is typical of unreinforced samples loaded perpendicular to grain. Samples with 6 mm nails were characterized by a wood fiber removal involving a larger and deeper area in comparison to samples with 4 mm nails, meaning that a connection using large diameter nails tends to cause more damage to the wood fiber substrate. Failure mode B (see Figure 4b) occurred to the reinforced specimens loaded according to both directions (parallel and perpendicular to grain), meaning that the skin reinforcement was able to reduce both the wood embedment and the material removal. As expected, this positive effect is more significant for samples loaded perpendicular to the grain. In fact, the 6 mm reinforced samples loaded along this direction showed an intermediate failure mode (B/C) characterized by a local

wood embedment associated with limited damage of the wood fiber substrate, instead of failure mode C typical of unreinforced specimens.

Concerning the failure mechanism of the nails used to connect the steel plate to the CLT panel shown in Figure 4d, it can be observed that two plastic hinges can be recognized into the nails, one in the shank (at a distance of about 2 times the nail diameter below the cap) and the other under the head, that causes the final failure of the nail at the wood panel – steel plate interface, typical of strengthened samples and unreinforced specimens with 4 mm nails.

A proper design of the number of nails adopted for the connections avoided brittle failures involving the fracture of the steel plates, which never occurred during the tests.

3.2. Force-slip curves

The experimental force-slip curves obtained from the tests are reported in Figure 5 and Figure 6 for monotonic and cyclic tests, respectively. In both figures, slip has to be intended as the averaged value of the steel plate – CLT panel slip displacements recorded by the 2 LVDTs used during the test. For a direct comparison, curves related to the unreinforced configuration (dashed blue lines) are superimposed to those coming from the reinforced configurations (solid black lines). In all the cases, a remarkable improvement due to the presence of reinforcement on the global behavior of the steel-to-CLT panel connection can be easily observed.

From the monotonic curves of Figure 5, it is possible to observe that the peak force values of the strengthened samples are always greater than the corresponding values of the unreinforced ones, irrespective of the grain orientation or of the nails diameters. In addition, slip values at peak are smaller for the reinforced specimens with respect to the unreinforced cases. Introduction of the reinforcement is also effective (Figure 5) in reducing the residual slips observed at the end of the first loading-unloading cycle in monotonic tests [35], thus improving the behavior under service conditions. Globally, the presence of the composite ply provides for a global stiffening of the load-slip curves for both the elastic and post-elastic (non-linear) branches. Finally, in the post-peak

phase, a softening regime can be observed due to the progressive failure of the nails leading to a stepwise curve for all the samples tested.

Comparing the curves of the samples loaded parallel to the grain with those loaded perpendicular to the grain, it can be observed that, regardless of the nail diameters and of the presence of the reinforcing ply, peak force values are usually lower for samples loaded along the second direction. Nevertheless, the reinforced samples are characterized by a lower dependency from the grain-load inclination if compared to the unreinforced ones, meaning that the composite ply, superficially glued to the CLT panel, tends to homogenize the wood behavior along the two orthogonal directions avoiding the local damage of the surface due to fiber removal and "locally reducing" the wood orthotropy. This behavior is perfectly aligned with the observed failure modes illustrated in Figure 4 and described in the previous section.

Cyclic force-slip curves illustrated in Figure 6 show a behavior qualitatively similar to the monotonic ones, since the strengthened samples are characterized by higher peak force, lower slip at peak and globally higher stiffness, if compared to the unreinforced ones. Samples fastened with 6 mm nails made an exception since, similarly to the monotonic tests, the peak slip seems to change only moderately due to reinforcement, meaning that the reinforcement is too weak to limit remarkably the nail slip in the post-yielding field. However, as for monotonic tests, the reinforcement is able to reduce the differences between the response of samples loaded along the two different directions (i.e. orthogonal and parallel to the grain).

If cyclic force-slip curves are compared to the corresponding monotonic ones, it is always possible to observe a general reduction of the peak force (10-12%) due to the small strength degradation observed for repeated cycles. Moreover, a reduction of the cyclic peak slip with respect to the monotonic one, can be observed for samples fastened with 4 mm nails, meaning that the reinforcement effectively reduces the nail slip in the post-elastic phase.

Concerning the cyclic behavior of the connections (Figure 6), it can be observed that the reinforcement keeps its effectiveness even under this type of condition with cycles which are almost

symmetric; both types of connections (reinforced and unreinforced) are characterized by a pinching effect, with a common value of residual force (at null slip) of about 5-10% of the peak one. The general strength degradation is small for all the specimens and it develops primarily during the first cycle repetition, followed by a rapid stabilization. It is worth noting that this behavior is common for composite strengthening systems [34].

4. ANALYSIS OF RESULTS AND DISCUSSION

In this section, results obtained from experimental tests are analyzed using suitable linearization methods in order to define the significant parameters characterizing the behavior of the investigated connection systems.

4.1. Linearization of experimental Load-Slip curves

Different methods are available in literature for the linearization of the experimental load-slip curves [37]. In general, two different approaches can be followed, that differ in the approximation level of the experimental load-slip curve. The first approach provides a refined approximation of the experimental curve using a multilinear backbone curve and is usually adopted for the development or for the calibration of numerical models. The second approach is simpler than the first one and is based on a bilinearization of the experimental load-slip curve, by using different methods for the definition of the yielding point [38-44]. This simplified approach can profitably be used for the bilinearization of experimental load-slip curves in order to make a comparison between the response of connections characterized by different experimental behaviors. Since the purpose of this work is to verify the effectiveness of a composite reinforcement to improve the behavior of a CLT-to-steel nailed connection, this last simplified approach has been adopted. It is worth noting that no unique procedure exists for the definition of the yielding point, therefore the adoption of different approaches could lead to quite different results [38].

In order to verify the influence of the linearization method on the values of parameters used to describe the response of the tested samples, three different approaches have been adopted and results have been compared. The method "b" of EN12512 (*EN-b*) [36] has been used at first to define the yielding points of the experimental load-slip curves since it is coherent with the adopted loading protocol. The corresponding results have been then compared with those obtained by using the Karacabeyli and Ceccotti method (*K*&*C*) [41] and the 5% diameter method (5%*d*) [40].

The *EN-b* method, in more detail, defines the yielding point as the intersection between the line with slope α, describing the initial elastic branch of the curve and the line with slope β=1/6 α that is imposed to be tangent to the experimental load-slip curve in the post-elastic branch. The slope α is that of the secant line passing through the points of the experimental curve located at 10% and 40% of the peak force [36]. Clearly, following this definition, the *EN-b* yielding point may not belong to the experimental load-displacement curve. On the contrary, the *K*&*C* and 5%*d* methods provide a yielding point belonging to the curve even if, like the *EN-b* method, they are based on conventional assumptions derived from the experimental observation of the nailed connections behavior.

In more details, the *K*&*C* method assumes the yielding point of the experimental curves as the point at the 50% of the peak load [41], while the 5%*d* method assumes the yielding point as the point of the experimental curve at a slip value equal to the 5% of the nail diameters [40].

For both methods, once the yielding point is defined, the bilinear backbone curve can be drawn by identifying a first elastic branch of slope K_1 (passing through the origin and the yielding point) and a second post-elastic branch of slope K_2 (passing through the yielding point and the peak point). Correspondingly, the parameters describing the bilinear backbone curve are: yielding displacement (d_y), yielding force (F_y), elastic (K_1) and post-elastic (K_2) stiffnesses.

For the different tests, the yielding point has been defined using the three presented methods in order to verify the possible influence of the linearization procedures in describing the response and discussing the results of the different configurations tested.

From this preliminary analysis (all the results are not reported here for lack of space), it was possible to observe that *EN-b* method generally provides the largest values of the yielding force F_y and displacement d_y, whereas *K&C* and 5%*d* methods provide, conversely, quite similar values of such parameters. Despite the yielding point obtained differs for the three different methods, values of the elastic stiffness K_1 are very similar, meaning that all the three linearization procedures are able to adequately capture the elastic stiffness of the tested samples. Moreover, the trend of variation of the bilinear backbone parameters, due for example to the variation of the load-grain orientation or the nail diameters or to the presence of the composite reinforcement, is also coherently captured by the three methods. Finally, a statistical analysis of the values associated to the different investigated parameters (F_y, d_y, K_1 and K_2), in terms of Coefficient of Variation (CoV), allowed to conclude that they are not directly influenced by the adopted linearization method.

This confirms that parameters describing the bilinear backbone curve can be properly defined by each one of the three methods presented in this work. Therefore, in the following, results will be presented and discussed only according to *EN-b* method, which is also consistent with the standard used for the experimental loading protocol.

The key parameters describing the backbone experimental curves and the load cycle at service conditions for the different configurations (grain-load inclination, nail diameters and test type) are summarized in Table 2. According to Figure 7, the backbone envelope is defined by the yielding point (d_y, F_y – circle), by the peak point ($d(F_{max})$, F_{max} – triangle) and by the failure point (d_u, F_u = 0.8 F_{max} – cross) for both monotonic and cyclic tests. Together with K_1 and K_2, the residual slip (d_r) at the end of the unloading phase and the secant stiffness (K_r) of the load cycle considered at the edge of the service condition (~0,40·F_{max}), for monotonic tests, the values of ductility (μ), defined as the ratio between the ultimate displacement d_u and the yielding slip d_y, are also reported in Table 2, for both monotonic and cyclic tests.

The mean values (mean) and the coefficient of variation (CoV) of such parameters are listed in Table 2 for all the eight tested configurations. The statistical scattering of the parameters is generally limited and the larger dispersion can be found for parameters of 6 mm nailed connections. As a general remark, the effect of the strengthening system is immediately evident, since it provides a significant increase of stiffness, capacity of the system and an overall reduction of the slip parameters. Furthermore, as a preliminary observation, cyclic loading always leads to a slight deterioration of the system, with a reduction of its maximum capacity (about 10%).

4.2. Effect of the reinforcement

In order to better analyze the effects of the reinforcement on the connections response, Figure 8 provides a comparison of the variation of the investigated mechanical parameters (X) between reinforced and unreinforced samples (X_{reinf}/X_{unr} -1).

Figure 8*a* shows the effect of the reinforcement on force parameters (peak force F_{max} and yielding force F_y): the applied composite ply has always resulted in a beneficial effect in increasing both force values for all test configurations. In more detail, the maximum force was found to be about 20% higher for samples with 4 mm nails loaded along direction parallel to grain (for both monotonic and cyclic tests) and orthogonal to grain (only for monotonic tests). The effect of reinforcement is more significant for samples with 4 mm nails loaded cyclically orthogonal to grain and for all the specimens with 6 mm nails, where the maximum force is about 35% higher if the sample is loaded parallel to grain and about 40% higher for the other grain-load inclination, regardless of the loading type (monotonic or cyclic). Yielding force F_y shows an increment more scattered if compared to F_{max}, even if a general trend with higher increments for cyclic tests can be identified. Moreover, the reinforcement effect on the yielding force seems more beneficial for cyclic tests performed on connections with 4 mm nails (40% - 50% range) if compared to cyclic tests on samples with 6 mm nails (about 30%). F_y variations under monotonic loading are much more comparable and are included in the 20-25% range for all the examined configurations. In general, the strengthening system provides a more significant performance increase for the samples

loaded orthogonal to grain. This conclusion is in perfect agreement with the identified failure modes, where a significant surface damage reduction was found in strengthened samples (see Figure 4*c* and 4*b*).

A general trend of reduction can be identified for different types of slips in all the tested configurations (Figure 8*b*). Slip at peak $d(F_{max})$ seems more reduced in the case of 4 mm nails and monotonic loading, while it is substantially unchanged in 6 mm nails configuration. The load-grain inclination does not seem to have an evident effect in this case.

Yielding slip is always reduced, due to the beneficial effect of reinforcement, with particular intensity for monotonic tests, where maximum reductions are 30 and 40%, respectively for 4 and 6 mm nails. Ultimate slip d_u seems to have a trend similar to slip at peak $d(F_{max})$. Additional considerations are possible for the residual slip d_r, evaluated only for monotonic tests, where a significant reduction (45-55%) can be found for all the tested configuration.

Finally, Figure 8c shows the effect of the reinforcement on elastic (K_1) and post-elastic (K_2) stiffness of the connection. Both stiffnesses are significantly improved by the surface strengthening system adopted: the first one (K_1) has been increased in the 60% - 100% range, regardless of the loading type and direction, except for N6_0-C configuration, where the increment is slightly lower (about 40%); the second one (K_2) has been improved in the same range with the exception of N4_0-C specimens.

4.3. Effect of the cyclic loading

In this section, the effect of the adopted loading protocol on the response of the system is evaluated for all the tested configurations.

Figure 9 provides a comparison of the variation of the investigated mechanical parameters (X) between cyclic and monotonic test results ($X_{cycl} / X_{mono} - 1$), in terms of relative difference (%).

Figure 9a shows the influence of the loading protocol (monotonic or cyclic) on force parameters (peak force F_{max} and yielding force F_y). Cyclic loading is found to reduce the maximum capacity of connections with 6 mm nails of about 10%, whereas the reduction for 4 mm nails is included in the

5-20% range. Considering unreinforced and strengthened samples of the same type, the effect of cyclic loading is sensibly reduced in connections with 4 mm nails with a more relevant effect for the samples loaded perpendicular to the grain. For samples fastened with 6 mm nails, the capacity degradation passing from monotonic to cyclic tests seems not to be, on average, influenced by the different load-to-grain inclination since the larger diameter limit the local damage around the nail under cyclic load.

If yielding force is analyzed, samples with smaller diameter nails are found to be more sensible to the type of loading, reducing the capacity during cyclic loading, while the load-grain inclination doesn't provide for a remarkable effect. In general, the cyclic loading produces less effects in strengthened samples under all the configurations tested (4 mm or 6 mm nails, 0° or 90°).

Figure 9b shows the comparison between monotonic and cyclic behavior of the connections in terms of displacements and ductility. Cyclic loading seems to have a limited effect on 6 mm nailed connections, while the influence is more noticeable in the case of 4 mm nails, where a reduction of about 40% was found for the yielding slip d_y. A lower variation was found for the ultimate slip d_u and for the slip $d(F_{max})$, thus leading to a general increased ductility (μ) under cyclic loading.

The effect of the type of loading on elastic and post-elastic stiffness is analyzed in Figure 9c: in connections with 6 mm nails the variation is reduced and included in the 20% range, whereas in 4 mm nailed connections cyclic loading provides a general stiffness increment, in particular for the elastic stiffness K_1.

As a general remark, connections with larger nails (6 mm) already under monotonic loading suffers of local damage, which is then less sensitive to cyclic loading, both in term of static and kinematic parameters.

4.4. Effect of the reinforcement on the cyclic behavior of the connection

According to EN 12512 [36], the cyclic behavior of the connection can be described by the strength degradation ΔF and by the equivalent viscous damping value ν_{eq}, evaluated at the end of each cycle

repetition. Specifically, the strength degradation was evaluated as the percentage difference between the force registered at the end of the second and third cycles and that achieved at the end of the first cycle [36]. On the other hand, the equivalent viscous damping represents the capability of the connection to dissipate energy and is defined as the ratio between the hysteretic dissipated energy, evaluated at each cycle repetition, and the energy representing the elastic behavior of the connection [36].

Table 3 reports, for the various positive (tension) and negative (compression) cycles, the strength degradation and the equivalent viscous damping values for all the tested samples. For sake of simplicity, these parameters are reported only for cycles with a maximum slip of $0{,}75 \cdot d_y$, d_y and $2 \cdot d_y$.

Analyzing the strength degradation values, it is possible to observe that, for all the specimens, values increase for increasing cycle amplitude. At the same time, the strength degradation is significant from the first to the second cycle repetition while it is much more limited from the second to the third cycle, meaning that capacity degradation tends to stabilize [34].

Concerning the equivalent viscous damping, a general reduction can be observed in strengthened samples, highlighting, as a negative effect, a reduction of the dissipative capability of the connection due to reinforcement. Nevertheless, it is worth noting that strengthening methods adopted for realizing hyper-resistant connections, in a hierarchy of resistances approach, are designed to produce low damage and high rigidity more than energy dissipation. The latter being localized in what is usually connected to them (hold-down, dampers, etc…).

5. COMPARISON WITH ANALYTICAL MODELS

The reference theory for the definition of the load-bearing capacity (i.e. slip moduli) of a nailed connection was firstly developed by Johansen [8] and later included in the design codes [23,45]. According to this theory, nailed joints have a range of possible failure mechanisms: embedment failure, bending failure or coupled effect. Embedment failure alone occurs if the timber or wood-

based material around the fastener is completely plasticized and the fastener remains straight. The key parameters for this failure mode are the embedment strength of the timber or wood-based material plus the joint geometry (thickness of the members to be connected, spacings, end- and edge-distances of the fasteners). Another failure mode affecting nailed joints is bending failure of the fastener with simultaneous embedment failure of the timber or wood-based material. When such combined failure occurs, one or two plastic hinges can be observed along the fastener, which is then inclined when crossing the area of the shear plane; this leads also to plastic embedment deformations. In this case, together with the previous embedment strength and joint geometry, yield bending moment of the fastener also are the key parameters governing the load-bearing capacity of the connection.

Equation 1 provides the mean load-bearing capacity (R_{v_J}) of a single nailed steel-to-timber joint (with thick steel plates) for the different described failure modes [8,46,47]:

$$R_{v\_J} = \min \begin{cases} f_h \cdot t_1 \cdot d & (a) \\ f_h \cdot t_1 \cdot d \left[\sqrt{2 + \dfrac{4 \cdot M_y}{f_h \cdot d \cdot t_1^2}} - 1 \right] & (b) \\ 1.4 \sqrt{2 \cdot M_y \cdot f_h \cdot d} & (c) \end{cases} \quad (1)$$

where f_h is the mean value of embedment strength, t_1 and d are, respectively, the fastener penetration depth and diameter, M_y is the mean values of fastener yielding moment. In detail, failure mode (*a*) of Equation 1 involves only the embedment of wood without plasticization of the nail that remains undeformed, while failure modes (*b*) and (*c*) are characterized by a simultaneous wood embedment and nail plasticization with the formation of a single or a couple of plastic hinges for mode (*b*) and (*c*) respectively. It is worth noting that, for the two ductile failure mechanisms (*b*) and (*c*) involving the formation of plastic hinges in the nail, the strength increases due to the so called "rope effect" (R_{ax}) which involves the withdrawal capacity of the nails [23]. This additional strength contribution is generally limited to the 50% of shear capacity R_{v_J} of the connection [23] (R_{ax} = 0.5 R_{v_J}). The load bearing capacity of the connection ($F_{Johansen}$) is therefore obtained by the sum of the two contribution R_{v_J} and R_{ax}.

The mean value of embedment strength (f_h) can be computed according to the formulation proposed by Blaß & Uibel [48] and reported in Equation 2:

$$f_h = 0.13 \cdot d^{-053} \cdot \rho^{1.05} \quad (2)$$

where ρ is the mean density value of the portion of wood-based material where the embedment phenomenon is localized. For unreinforced connections, timber density was obtained with experimental tests according to EN 384 [27]. The mean value of the fastener yielding moment was instead experimentally determined according to EN 409 [30].

The elastic stiffness of the connection (k_{ser}) can be reliably predicted by using the formulation proposed by Eurocode 5 [23] and reported in Equation 3:

$$k_{ser} = \rho^{1.5} \cdot d^{0.8}/30 \quad (3)$$

Finally, due to the large spacing between nails, no reduction effects (interaction between nails) are considered to compute the overall lateral capacity ($F_{Johansen}$) and stiffness (K_{ser}) of the connection, which is then obtained by multiplying the resistance and stiffness of each single nail by the number of them (n) used in the connection [49].

It is worth noting that both the load-bearing capacity and the stiffness of the connection increase if the density ρ and therefore the embedment strength of wood or wood-based material increases. Interventions that locally increase these parameters, such as reinforcement realized with nail-plate connectors [20,21] or reinforcement applied in the form of glued-on high density wood-based panels [22] or glued on FRP plies, allow to significantly increase both the load bearing capacity and the stiffness of the connection.

Different approaches have been developed by many researchers to compute the load bearing capacity of connection with local improvement of the embedment strength [2,50]. These approaches are based on a reformulation of the Johansen equations reported in Equation 1, since they consider modified failure modes due to presence of the high strength/density layer.

The model developed by Blaß et al. [2] proposes the reformulation of the Johansen equations according to Equation 4:

$$R_{v\_B} = \min \begin{cases} f_{h,CLT} \cdot t_1 \cdot d + f_{h,s} \cdot s \cdot d & (a) \\ f_{h,CLT} \cdot d \left[\sqrt{2 \cdot t_1^2 + 2 \cdot (1-\eta) \cdot s^2 + 4 \cdot s \cdot t_1 + \frac{4 \cdot M_y}{f_{h,CLT} \cdot d}} - (t_1 + 2 \cdot s) \right] + f_{h,s} \cdot s \cdot d & (b) \\ f_{h,CLT} \cdot d \left[\sqrt{(1-\eta) \cdot s^2 + \frac{4 \cdot M_y}{f_{h,CLT} \cdot d}} - s \right] + f_{h,s} \cdot s \cdot d & (c) \end{cases} \quad (4)$$

where $f_{h,CLT}$ is the embedment strength of CLT, $f_{h,s}$ is the embedment strength of the reinforcement (experimentally evaluated according to EN 383 [51]), s is the reinforcement thickness and η is the embedment strengths ratio ($f_{h,s}/f_{h,CLT}$). According to this approach, Equation 1 is a particular case of Equation 4 which can be obtained neglecting the reinforcement contribution ($f_{h,s} = 0$ and $s = 0$). As for the reference Johansen model, for the two ductile failure mechanisms (*b*) and (*c*) involving the formation of plastic hinges in the nail, the strength increases due to the so called "rope effect" (R_{ax}) has to be accounted and limited to the 50% of shear capacity of the connection [23]. The load bearing capacity of the connection according to the Blaß model ($F_{Blaß}$) is therefore obtained by the sum of the two contribution R_{v_B} and R_{ax}.

Despite the good capacity of representing the physical phenomenon involved, this method is highly complex since it requires the introduction, for each possible reinforcement configuration, of specific equations that are not typically used by practitioners in the design of the connections.

In this work, a specification of the reference formulations reported in Equation 1 for the calculation of connection load-bearing capacity and stiffness is proposed, to account for the experimentally observed strength and stiffness increment due to the FRP skin reinforcement. The strengthening effect has been accounted for simply by using a modified *improved density value* (ρ) inside the general formulations previously adopted for strength and stiffness calculation. In more detail, the modified density (ρ) has been defined as the weighted average of the densities of materials involved in the connection, properly taking into account the different thicknesses of the layers according to Equation 5:

$$\rho = \frac{(\rho_t \cdot s_t + \rho_e \cdot s_e + \rho_{CLT} \cdot s_{CLT})}{(s_t + s_e + s_{CLT})} \quad (5)$$

where ρ_t and s_t are, respectively, the dry carbon fabric density and thickness, ρ_e and s_e are, respectively, the adhesive density and thickness, ρ_{CLT} and s_{CLT} are, respectively, the mean density and thickness of the CLT panel where the wood embedment phenomenon is localized. From the experimental tests conducted in this work and other available in literature [52], it was possible to observe that this thickness is about twice the nail diameter, therefore $s_{CLT} = 2d$. The value of the parameters adopted for the calculation of the load bearing capacity, according to the two models ($F_{Johansen}$ and $F_{Blaß}$) and stiffness (K_{ser}) of the unreinforced and strengthened connections are reported in Table 4. According to code recommendations, for small diameter nails the load bearing capacity is not affected by load-grain direction.

Analyzing the density values reported in Table 4 for the different configurations, it is possible to observe that for all the unreinforced samples the mean density value is 438 kg/m^3, while for 4 mm and 6 mm diameter reinforced samples the density values are significantly increased of about 68% and 50%, respectively. The percentage increment of the embedment strength due to the reinforcement is about 72% for 4 mm samples and 54% for 6 mm samples. These strength increments are coherent with those obtained from experimental tests shown in Figure 8a and reported in Table 5, together with the analytical predictions of the strength, obtained with Johansen and Blaß models ($F_{Johansen}$ and $F_{Blaß}$), and stiffness ($K_{ser,\ model}$) values.

Comparison between the proposed model, based on the Johannsen equations with modified (improved) density, and the alternative one proposed by Blaß et al. [2] is reported in Table 5 in terms of absolute values and percentage errors. For both the models, the minimum strength value is achieved with the failure mode “c” (double plastic hinge along the nail shank), that is perfectly coherent with the experimental evidence.

Comparison between analytical and experimental results allows to verify the reliability of the proposed analytical models in predicting the strength and elastic stiffness values. When considering the unreinforced CLT nailed connections, both the analytical models, in general, slightly underestimates the mean experimental values, according to [46], and the errors are limited.

The model proposed by Blaß et al. [2] provides generally higher values of resistance, with a difference which is limited for strengthened connections with 4 mm nails and larger for 6 mm nails. Both the models tend to overestimate the strength of the 4 mm samples loaded perpendicular to the grain. The percentage difference between the two analyzed models is always limited and equal to 6.5 % for 4 mm nails and to 15% for 6 mm nails, respectively.

Errors provided by the proposed model are, anyway, always limited and suggest a greater accuracy for strengthened connections with 4 mm nails, whereas, for reinforced connections with 6 mm nails, the two models don't always show a clear trend, with the proposed analytical model that seems to be on the safe side in predicting experimental outcomes and, for this reason, more suitable for design purposes.

The proposed model, although based on the simple correction of the density value, succeeds in satisfactorily predicting the effect of the reinforcement.

Concerning the stiffness values, the analytical model captures quite well the experimental response both for unreinforced and reinforced configurations even if the errors are generally greater than those of strength values. Nevertheless, it is worth noting that the theme of the correct prediction of the connection stiffness is still an open issue on which many researchers are currently working [53].

6. CONCLUSIONS

The paper presents the results of an extensive experimental campaign focusing on the investigation of the effects of a local FRP reinforcement, applied with the aim of realizing hyper-resistant connections, on the behavior of steel-to-CLT nailed joints.

Results show a beneficial effect of the strengthening system, based on a multiaxial carbon fabric applied with epoxy resin, on the connection behavior with increased load-bearing capacity and stiffness in both monotonic and cyclic tests. Failure mode involving wood embedment and wood fiber removal are also improved by the reinforcement, especially when samples are loaded perpendicular to the grain. Experimental curves have been analyzed according to proper

linearization methods, that allow to define the reinforcement effect in terms of strength and stiffness parameters, concluding that the reinforcement effect is not dependent from the adopted linearization method.

According to the chosen EN 12512 – "b method" linearization technique, which is also coherent with the adopted loading protocol, the effect of the strengthening system is found to be significant in increasing load-bearing capacity and stiffness of the nailed connection, for each tested configuration. In more detail, the reinforcement is able to increase both the maximum force and the yielding force of the connection and leads to a general reduction of displacement parameters, allowing for a remarkable increase of elastic and post-elastic stiffness, independently from load-grain inclination. This analysis allows to conclude that the proposed strengthening system can be successfully used for realizing a light and efficient hyper-resistant connection.

The effect of cyclic loading is also analyzed, concluding that a general reduction of the maximum capacity has to be expected after cycles repetition. The capacity degradation registered after the first cycle repetition tends to stabilize as the number of cycles increases and an overall 15% reduction seems to be a realistic final estimate.

Finally, a simple analytical model based on the reference theory proposed by the current standards has been developed for predicting the load-bearing capacity and stiffness of unreinforced and strengthened samples, obtaining results in good agreement with experimental outcomes and with results assessed with more refined models available in literature.

7. ACKNOWLEDGEMENTS

The financial support of TIRISICO Project (POR FESR 2014-2020 – Regione Emilia Romagna) and of (Italian) Department of Civil Protection (ReLUIS 2019-2021 Grant – Innovative Materials) are gratefully acknowledged. The Authors would like also to thank the partner companies Vibro-Bloc S.p.A. and Fibrenet S.p.A. for their support and Dr. Gianluca Ussia and Dr. Francesco Grandi for the kind cooperation.

REFERENCES

[1] Izzi M, Casagrande D, Bezzi S, Pasca D, Follesa M, Tomasi R. Seismic behaviour of Cross-Laminated Timber structures: a state-of-the-art review. Eng Struct 2018;170:42-52.

[2] Blaß HJ, Schädle P. Ductility aspects of reinforced and non-reinforced timber joints. Engineering Structures 2011;33(11):3018-3026.

[3] Izzi M, Polastri A, Fragiacomo M. Investigating the hysteretic behavior of cross-laminated timber wall systems due to connections. J Struct Eng 2018;144(5):04018035.

[4] Trutalli D, Marchi L, Scotta R, Pozza L. Capacity design of traditional and innovative ductile connections for earthquake resistant CLT structures. Bulletin of Earthquake Engineering 2018. In press. https://doi.org/10.1007/s10518-018-00536-6.

[5] Scotta R, Marchi L, Trutalli D, Pozza L.A dissipative connector for CLT buildings: concept, design and testing. Materials 2016;9(3):139. MDPI. DOI:10.3390/ma9030139.

[6] Latour M, Rizzano G. Cyclic behavior and modeling of a dissipative connector for cross-laminated timber panel buildings. J. Earthq. Eng. 2015;19:137–171.

[7] Polastri A, Giongo I, Piazza M. An innovative connection system for cross-laminated timber structures. Struct Eng Int 2017;27:502–511.

[8] Johansen KW. Theory of timber connections. In: *Int. assoc. bridg. struct. eng.*, Bern, Switzerland, 1949. p. 249–62.

[9] Plevris N, Triantafillou TC. FRP-reinforced wood as structural material. *J Mater Civil Eng* 1992;4:300-317.

[10] Triantafillou TC. Shear reinforcement of wood using FRP materials. ASCE J Mater Civil Eng 1997;9(2):65-69.

[11] Schober K-U, Harte AM, Kliger R, Jockwer R, Xu Q, Chen J-F. FRP reinforcement of timber structures. Construction and Building Materials 2015;97:106-118.

[12] Vahedian A, Shrestha R, Crews K. Effective bond length and bond behaviour of FRP externally bonded to timber. Construction and Building Materials 2017;151:724-754.

[13] Gomez EP, Gonzales MN, Hosokawa K, Cobo A. Experimental study of the flexural behavior of timber beams reinforced with different kinds of FRP and metallic fibers. Composite Structures 2019;213:308-316.

[14] Soltis LA, Ross RJ, Windorski DF. Fiberglass-reinforced bolted wood connections. Forest Products Journal 1198;48:63-67.

[15] Hollaway LC, Teng JG. Strengthening and rehabilitation of civil infrastructures using fibre-reinforced polymer (FRP) composites, vol. 25. Cambridge, England: Woodhead Publishing Limited, Great Abington, 2008.

[16] Triantafillou TC. Composites: a new possibility for the shear strengthening of concrete, masonry and wood. Compos Sci Technol 1998;58:1285-1295.

[17] Mazzotti C, Ferracuti B, Bellini A. Experimental bond tests on masonry panels strengthened by FRP. Composites Part B 2015;80:223-237.

[18] de Felice G, Aiello MA, Bellini A, Ceroni F, De Santis S, Garbin E, Leone M, Lignola GP, Malena M, Mazzotti C, Panizza M, Valluzzi MR 2016. Experimental characterization of composite-to-brick masonry shear bond. Materials and Structures 2016;49:2581-2596.

[19] Mazzotti C, Murgo FS. Numerical and experimental study of GFRP-masonry interface behavior: Bond evolution and role of the mortar layers. Composites Part B 2015;75:212-225.

[20] Kevarinmäki A, Kangas J, Nokelaiken T, Kanerva P. Nail-plate reinforced bolt joints of Kerto-FSH structures. 1995. Publication 51, Helsinki University of Technology.

[21] Blaß HJ, Schmid M. Verstärkung von Verbindungen. Bauen mit Holz 2001;103:40-48.

[22] Blaß HJ, Werner H. Stabdübelverbindungen mit verstärkten Anschlussbereichen. Bauen mit Holz 1988;90:601-607.

[23] Eurocode 5 – design of timber structures, Part 1–1: General – Common rules and rules for buildings. European Committee for Standardization (CEN). 2009.

[24] EN338. Structural timber. Strength classes. Brussels, Belgium: CEN. 2009.

[25] ETA-12/0281. CLT – Cross Laminated Timber: Solid wood slab elements to be used as structural element in buildings. Brussels, Belgium: European Organisation for Technical Approvals. 2011.

[26] EN 1380. Timber structures. Test methods. Load bearing nails, screws, dowels and bolts. Brussels, Belgium: CEN. 2009.

[27] EN 384. Structural timber – Determination of characteristics values of mechanical properties and density. Brussels, Belgium: CEN. 2016.

[28] ETA-04/0013. Nails and screws for use in nailing plates in timber structures. Brussels, Belgium: European Organisation for Technical Approvals. 2015.

[29] Eurocode 3 – Design of steel structures, Part 1-1: General rules and rules for buildings. European Committee for Standardization (CEN). 2005.

[30] EN 409. Timber structures – Test methods – Determination of the yield moment of dowel type fastners. Brussels, Belgium: CEN. 2009.

[31] ISO 1183-1. Plastics - Methods for determining the density of non-cellular plastics – Part 1: Immersion method, liquid pycnometer method and titration method. ISO/TC 61/SC5 Physical-chemical properties. 2019

[32] ISO 1675. Plastics – Liquid resins – Determination of density by the pycnometer method. ISO/TC 61/SC5 Physical-chemical properties. 1985.

[33] Bellini A, Bovo M, Mazzotti C. Experimental and numerical evaluation of fiber-matrix interface behaviour of different FRCM systems. Composites Part B 2019;161:411-426.

[34] Bellini A, Shahreza SK, Mazzotti C. Cyclic bond behavior of FRCM composites applied on masonry substrate". Composites Part B 2019;169:189-199.

[35] EN 26891. Timber structures. Joints made with mechanical fasteners. General principles for the determination of strength and deformation characteristics. Brussels, Belgium: CEN. 1991.

[36] UNI EN 12512. Timber structures. Test methods. Cyclic testing of joints made with mechanical fasteners. UNI. 2006.

[37] Pozza L, Saetta A, Savoia M, Talledo D. Coupled axial-shear numerical model for CLT connections. Construction and Building Materials 2017;150:568-582.

[38] Muñoz W, Mohammad M, Salenikovich A, Quenneville P. Determination of yield point and ductility of timber assemblies: in search for a harmonised approach. Proceedings of Int. counc. res. innov. build. constr. CIB-W18, 2008. p. 42–12–2.

[39] ASTM E 2126-05. Standard Test Method for Cyclic (Reversed) Load Test for Shear Resistance of Walls for Buildings. American Society for Testing and Materials (ASTM). West Conshohocken, PA, USA. 2005.

[40] ASTM D 5764-97a. Standard Test Method for Evaluating Dowel-Bearing Strength of Wood and Wood-Based Products. American Society for Testing and Materials (ASTM). West Conshohocken, PA, USA. 2005.

[41] Karacabeyli E, Ceccotti A. Quasi-static reversed cyclic testing of nailed joints. Proceedings of International Council for Building and Research Studies and Documentation Working Commission W18 – Timber Structures, 1996. Pap. 29–7–7.

[42] Ceccotti A. Timber connections under seismic actions. In: Timber engineering-STEP 1. 1st Edition. STEP/EUROFORTECH. The Netherlands. 1995. ISBN 90-5645-001-08. Pp. C17/1-C17/10.

[43] Yasumura M, Kawai N. Estimating seismic performance of wood-framed structures. Proceedings of 1998 I.W.E.C. Switzerland. 1998. Vol.2. pp. 564-571.

[44] Commonwealth Scientific and Industrial Research Organization (CSIRO). Timber evaluation of mechanical joint systems. Part 3, Earthquake loading. CSIRO, Melbourne, Australia. 1996.

[45] CNR-DT 206 R1/2018. Istruzioni per la Progettazione, l'Esecuzione ed il Controllo delle Strutture di Legno. 2018. [in Italian].

[46] Pozza L, Ferracuti B, Massari M, Savoia M. Axial-shear interaction on CLT hold-down connections – Experimental investigation. Engineering Structures 2018; 160: 95-110.

[47] Hilson BO. Joints with dowel-type fasteners. In: Theory, Timber engineering STEP 1: Basis of the design, material properties, structural components and joints, Centrum Hout, Almere, The Netherlands; 1995. p. C3/1-11.

[48] Blaß HJ, Uibel T. Load carrying capacity of joints with dowel type fasteners in solid wood panels. In: Int. counc. res. innov. build. constr., CIB-W18, 2006. p. 39–7–5.

[49] Izzi M, Flatscher G, Fragiacomo M, Schickhofer G. Experimental investigations and design provisions of steel-to-timber joints with annular-ringed shank nails for Cross–Laminated Timber structures. Construction and Building Materials 2016;122:446-57.

[50] Haller P, Wehsener J, Chen CJ. Development of joints by compressed wood and glassgrain reinforcement. COST C1 – Control of the semi-rigid behaviour of civil engineering connections, International Conference, Liège. 1998.

[51] EN 383. Timber structures – Test methods – Determination of embedment strength and foundation values for dowel type fasteners. Brussels, Belgium: CEN. 2007.

[52] Pozza L, Savoia M, Saetta A, Talledo D. Angle bracket connections for CLT structures: Experimental characterization and numerical modelling. Construction and Building Materials 2018;91:95-113.

[53] Polastri A, Pozza L. Proposal for a standardized design and modeling procedure of tall CLT buildings. Int J Quality Res 2016;10(3):607-624. http://dx.doi.org/10.18421/IJQR10.03-12.

Table 1. Experimental campaign and observed failure modes.

Group ID	Number of tests	Type of connection	Load / grain inclination	Reinforcement	Type of test	Failure mode
N4_0-M	5	12 × 4×60 A. N.	0°	NO	Monotonic	A
N4_90-M	5	12 × 4×60 A. N.	90°	NO	Monotonic	C
N4E_0-M	5	12 × 4×60 A. N.	0°	YES	Monotonic	B
N4E_90-M	5	12 × 4×60 A. N.	90°	YES	Monotonic	B
N6_0-M	5	8 × 6×60 A. N.	0°	NO	Monotonic	A
N6_90-M	5	8 × 6×60 A. N.	90°	NO	Monotonic	C
N6E_0-M	5	8 × 6×60 A. N.	0°	YES	Monotonic	B
N6E_90-M	5	8 × 6×60 A. N.	90°	YES	Monotonic	B/C
N4_0-C	5	12 × 4×60 A. N.	0°	NO	Cyclic	A
N4_90-C	5	12 × 4×60 A. N.	90°	NO	Cyclic	C
N4E_0-C	5	12 × 4×60 A. N.	0°	YES	Cyclic	B
N4E_90-C	5	12 × 4×60 A. N.	90°	YES	Cyclic	B
N6_0-C	5	8 × 6×60 A. N.	0°	NO	Cyclic	A
N6_90-C	5	8 × 6×60 A. N.	90°	NO	Cyclic	C
N6E_0-C	5	8 × 6×60 A. N.	0°	YES	Cyclic	B
N6E_90-C	5	8 × 6×60 A. N.	90°	YES	Cyclic	B/C

Table 2. Experimental results: mean and CoV values of the mechanical parameters describing the response of the samples tested.

			N4_0	N4E_0	N4_90	N4E_90	N6_0	N6E_0	N6_90	N6E_90
F_y [kN]	M	Mean	31.79	38.99	28.40	36.13	41.32	49.98	36.97	44.41
		CoV	3.14%	5.46%	12.47%	4.61%	14.57%	8.79%	9.20%	7.36%
	C	Mean	24.01	33.38	21.31	32.30	38.27	48.29	34.01	44.96
		CoV	13.45%	4.39%	1.73%	11.16%	4.39%	6.03%	11.29%	7.40%
F_{max} [kN]	M	Mean	41.42	49.08	39.03	46.12	53.61	70.90	47.54	66.47
		CoV	4.34%	5.65%	5.44%	4.05%	12.55%	9.52%	3.23%	2.19%
	C	Mean	35.26	43.61	32.05	44.16	48.41	66.18	43.33	60.46
		CoV	6.02%	2.59%	3.11%	5.53%	5.48%	5.36%	8.43%	8.90%
d_r [mm]	M	Mean	0.84	0.48	0.70	0.38	1.53	0.69	1.06	0.55
		CoV	5.64%	15.95%	12.60%	7.16%	14.06%	10.30%	7.21%	9.80%
d_y [mm]	M	Mean	2.38	1.76	2.16	1.54	4.27	2.62	3.32	2.10
		CoV	2.64%	10.22%	17.42%	5.82%	8.79%	11.33%	18.06%	14.83%
	C	Mean	1.29	1.06	1.08	0.91	3.67	3.37	3.08	2.51
		CoV	19.77%	18.94%	14.95%	6.00%	9.12%	13.92%	18.83%	9.99%
$d(F_{max})$ [mm]	M	Mean	7.96	4.80	7.82	4.65	15.22	12.33	11.27	12.20
		CoV	17.80%	14.40%	18.01%	14.77%	4.74%	11.38%	8.37%	17.61%
	C	Mean	5.69	4.19	5.55	3.79	15.18	13.82	11.01	11.13
		CoV	9.41%	14.09%	9.07%	18.70%	3.60%	4.11%	23.27%	18.34%
d_u [mm]	M	Mean	10.27	6.09	9.87	6.19	21.99	17.74	15.00	13.98
		CoV	6.25%	7.44%	11.16%	10.62%	9.70%	21.97%	5.01%	12.99%
	C	Mean	7.28	5.17	6.65	4.84	20.95	20.61	15.10	15.09
		CoV	9.51%	5.05%	7.92%	16.81%	12.38%	9.54%	33.98%	28.91%
μ [–]	M	Mean	4.32	3.49	4.66	4.06	5.17	6.84	4.69	6.86
		CoV	8.58%	10.87%	17.93%	15.00%	9.02%	23.90%	26.11%	28.59%
	C	Mean	5.85	5.01	6.25	5.35	5.70	6.24	4.97	6.13
		CoV	25.71%	16.28%	15.59%	15.91%	5.70%	20.78%	35.41%	34.67%
K_1 [kN/mm]	M	Mean	13.37	22.40	13.31	23.57	9.64	19.23	11.30	21.40
		CoV	2.09%	12.11%	11.53%	6.70%	7.68%	12.78%	10.93%	11.80%
	C	Mean	18.77	32.24	20.03	35.72	10.48	14.45	11.31	18.04
		CoV	8.86%	14.52%	13.13%	11.61%	6.84%	8.79%	18.42%	12.46%
K_2 [kN/mm]	M	Mean	1.76	3.35	1.91	3.22	1.13	2.21	1.34	2.24
		CoV	14.06%	17.23%	10.48%	9.68%	11.86%	25.42%	14.50%	16.50%
	C	Mean	2.57	3.33	2.42	4.21	0.88	1.71	1.21	1.88
		CoV	5.95%	12.46%	10.03%	13.46%	17.81%	5.38%	15.18%	25.74%
K_r [kN/mm]	M	Mean	101.14	109.59	42.72	70.87	88.69	118.22	35.07	80.00
		CoV	12.99%	21.05%	11.02%	9.96%	25.32%	19.15%	18.60%	36.81%

Table 3. Strength degradation (ΔF) and equivalent viscous damping values (ν_{eq}) at different cyclic amplitudes for the tested samples.

		0.75d_y				***d_y***				**2d_y**			
		Tension		**Compression**		**Tension**		**Compression**		**Tension**		**Compression**	
		2nd	**3rd**	**2nd**	**3rd**	**2nd**	**3rd**	**2nd**	**3rd**	**2nd**	**3rd**	**2nd**	**3rd**
N4_0-C	**ΔF**	9.60	12.80	10.25	12.49	11.70	15.58	11.57	13.75	-	-	-	-
	ν_{eq}	8.75	7.62	8.48	7.65	9.79	8.43	9.51	8.63	-	-	-	-
N4E_0-C	**ΔF**	9.72	14.30	11.09	15.92	13.56	17.14	12.98	14.98	-	-	-	-
	ν_{eq}	7.70	6.77	7.13	6.26	8.02	6.91	7.46	6.87	-	-	-	-
N4_90-C	**ΔF**	6.78	9.71	5.85	8.37	7.15	10.26	6.03	8.46	-	-	-	-
	ν_{eq}	7.47	6.61	7.15	6.42	9.04	7.97	8.87	8.04	-	-	-	-
N4E_90-C	**ΔF**	8.41	11.02	10.65	13.04	10.36	14.00	8.62	12.24	-	-	-	-
	ν_{eq}	6.17	5.55	5.88	5.19	6.76	5.84	6.75	5.66	-	-	-	-
N6_0-C	**ΔF**	16.27	20.80	13.74	15.51	14.70	18.73	10.87	14.17	22.36	31.92	17.45	22.07
	ν_{eq}	6.69	6.14	6.50	5.94	6.33	5.61	6.35	5.79	9.11	5.81	7.83	6.05
N6E_0-C	**ΔF**	13.55	19.34	12.75	16.18	16.67	21.64	16.18	18.54	17.09	25.09	19.98	22.83
	ν_{eq}	7.46	6.60	6.81	6.04	6.45	5.54	5.85	5.31	7.54	5.42	6.49	5.49
N6_90-C	**ΔF**	11.24	15.05	7.50	10.82	10.83	13.64	7.86	11.56	13.28	18.17	12.05	16.38
	ν_{eq}	6.70	6.38	6.65	5.86	6.23	5.60	6.21	5.54	6.95	5.26	6.39	5.28
N6E_90-C	**ΔF**	10.09	13.88	8.66	11.61	12.29	17.38	10.59	12.75	16.72	23.85	14.54	18.92
	ν_{eq}	7.68	6.88	7.16	6.38	6.87	6.05	6.59	6.05	7.08	5.39	7.07	6.00

Table 4. Adopted parameters for computing the load-bearing capacity and the stiffness of unreinforced and strengthened samples according to the proposed models.

Parameter	**N4**	**N4E**	**N6**	**N6E**
number of nails (n)	12		8	
d [mm]	4		6	
t_1 [mm]	54.00	50.44	54.00	50.44
M_y [N mm] (EN 409 [30])	8282.46		27840.19	
ρ_{CLT} [kg/m^3] (EN384 [27])	438			
s_{CLT} = 2d [mm]	-	8	-	12
$f_{h,CLT}$ [MPa]	37.02		29.86	
ρ_t [kg/m^3] (ISO 1183-1 [31])	-	1780	-	1780
s_t [mm]	-	0.056	-	0.056
ρ_e [kg/m^3] (ISO 1675 [32])	-	1400	-	1400
s_e [mm]	-	3.50	-	3.50
$f_{h,s}$ [MPa] (EN 383 [51])	-	106.30	-	106.30
s [mm]	-	3.556	-	3.556
Proposed model (Eq. 1)				
ρ [kg/m^3] (Eq. 5)	438.00	735.87	438.00	659.27
f_h [MPa] (Eq. 2)	37.02	63.83	29.86	45.87
R_{v_J} (single nail)* [kN]	2.19	2.88	4.42	5.48
R_{ax} (single nail) [kN]	1.10	1.44	1.64	2.13
k_{ser} (single nail) [kN/mm] (Eq. 3)	0.93	2.02	1.28	2.37
Blaß model (Eq. 4)				
$\eta = f_{h,s} / f_{h,CLT}$	-	2.87	-	3.56
R_{v_B} (single nail)* [kN]	2.19	3.08	4.42	5.98
R_{ax} (single nail) [kN]	1.10	1.54	1.64	2.98
* minimum value from equation 1 and 4 – failure mode "c"				

Table 5. Comparison between experimental and analytical strength and stiffness values.

	$F_{exp,mean}$ [kN]	$F_{Johansen}$ [kN] (err. %)	$F_{Blaß}$ [kN] (err. %)	$(F_{Johansen} - F_{Blaß})/F_{Blaß}$ [%]	$K_{exp,mean}$ [kN/mm]	$K_{ser,model}$ [kN/mm] (err. %)
N4_0-M	41.42	39.47 (-4.72%)		-	13.37	11.12 (-16.86%)
N4_90-M	39.03	39.47 (1.12%)			13.31	11.12 (-16.49%)
N4E_0-M	**49.08**	**51.82 (+5.59%)**	**55.44 (+12.95%)**	**-6.52%**	**22.40**	**24.21 (+8.06%)**
N4E_90-M	**46.12**	**51.82 (+12.37%)**	**55.44 (+20.20%)**		**23.57**	**24.21 (+2.69%)**
N6_0-M	53.61	48.52 (-9.50%)		-	9.64	10.25 (6.32%)
N6_90-M	47.54	48.52 (2.05%)			11.30	10.25 (-9.30%)
N6E_0-M	**70.90**	**60.87 (-14.14%)**	**71.76 (1.21%)**	**-15.17%**	**19.23**	**18.93 (-1.57%)**
N6E_90-M	**66.70**	**60.87 (-8.74%)**	**71.76 (+7.58%)**		**21.40**	**18.93 (-11.55%)**

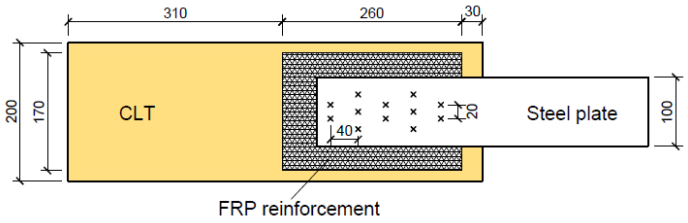

(*a*)

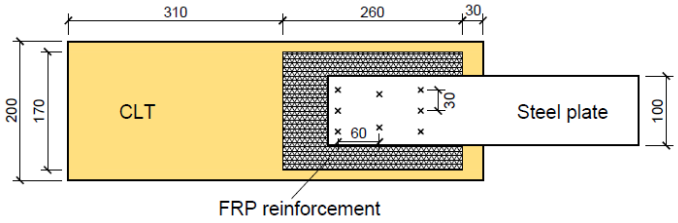

(*b*)

Figure 1. Specimens: (*a*) 4×60 A.N. connections and (*b*) 6×60 A.N. connections.

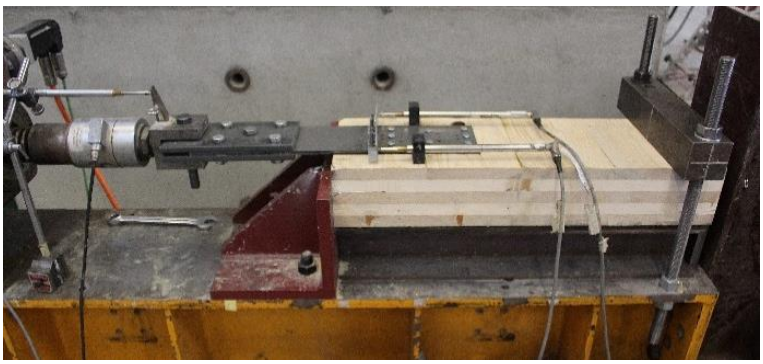

(*a*)

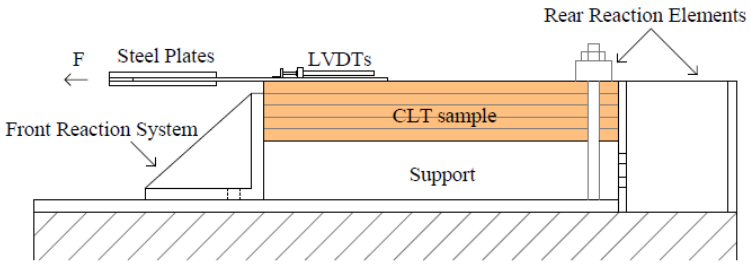

(*b*)

Figure 2. Test set-up: (*a*) global view and (*b*) geometry and details.

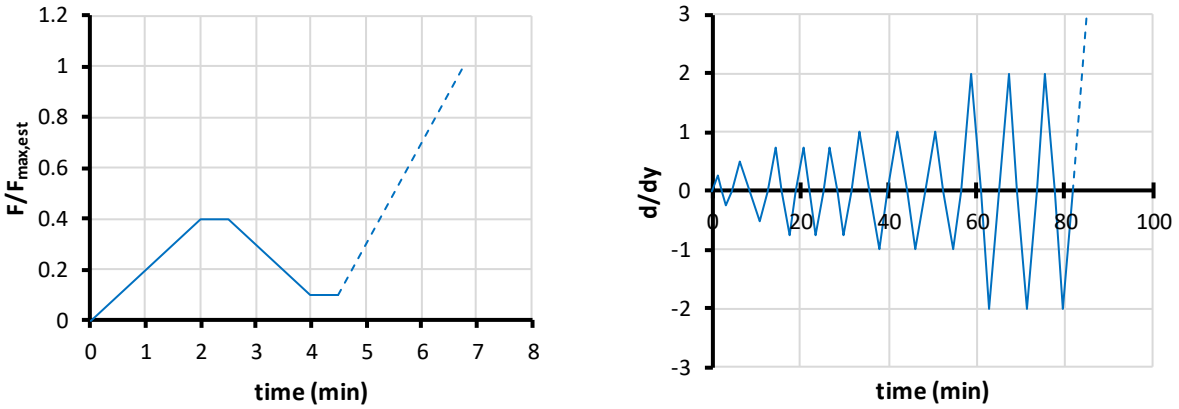

(*a*) (*b*)

Figure 3. Load protocol: (*a*) monotonic tests; (*b*) cyclic tests.

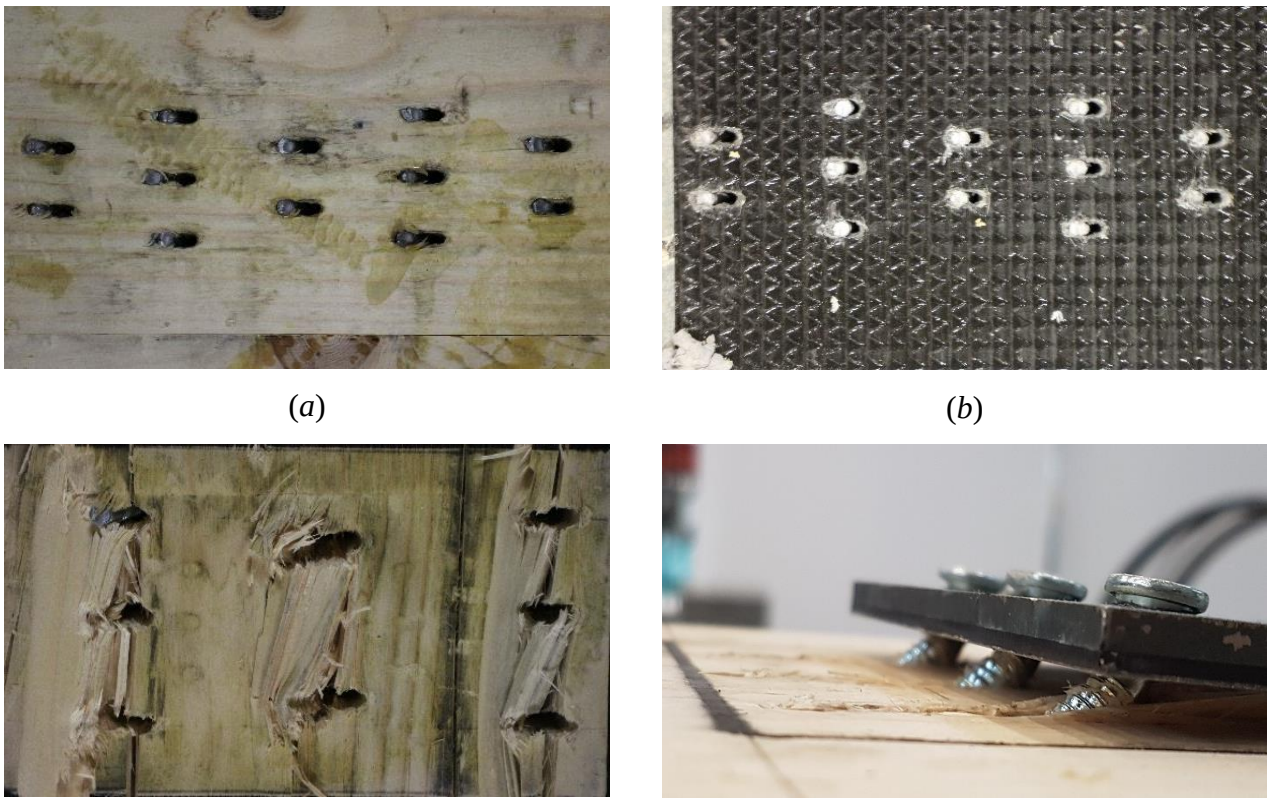

(*a*) (*b*)

(*c*) (*d*)

Figure 4. Failure modes identified during the tests: (*a*) Failure mode A (embedment); (*b*) Failure mode B (reduced embedment); (*c*) Failure mode C (embedment with surface damage); (*d*) Detail of the deformed nail at the end of the test.

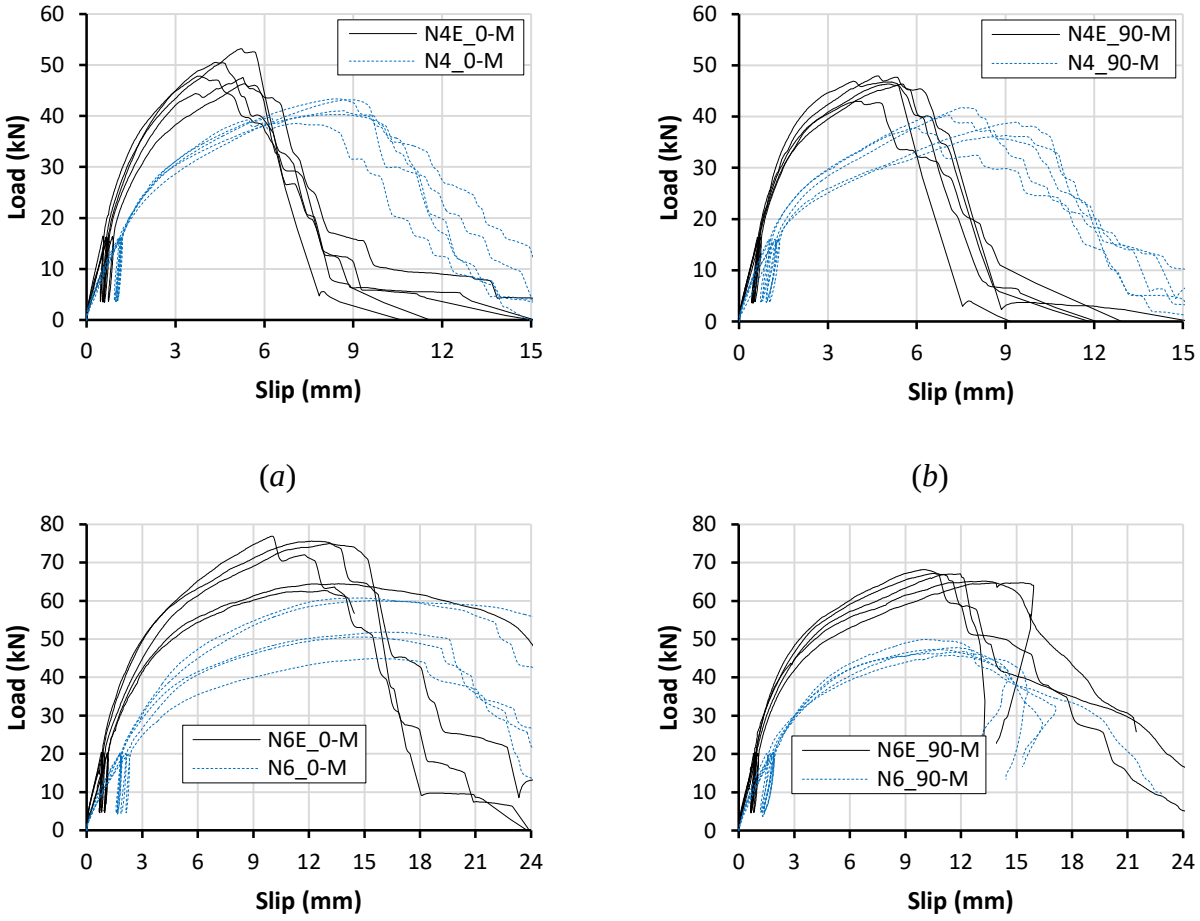

Figure 5. Experimental monotonic force-slip curves of unreinforced samples (dashed blue lines) superimposed to strengthened samples (continuous black lines).

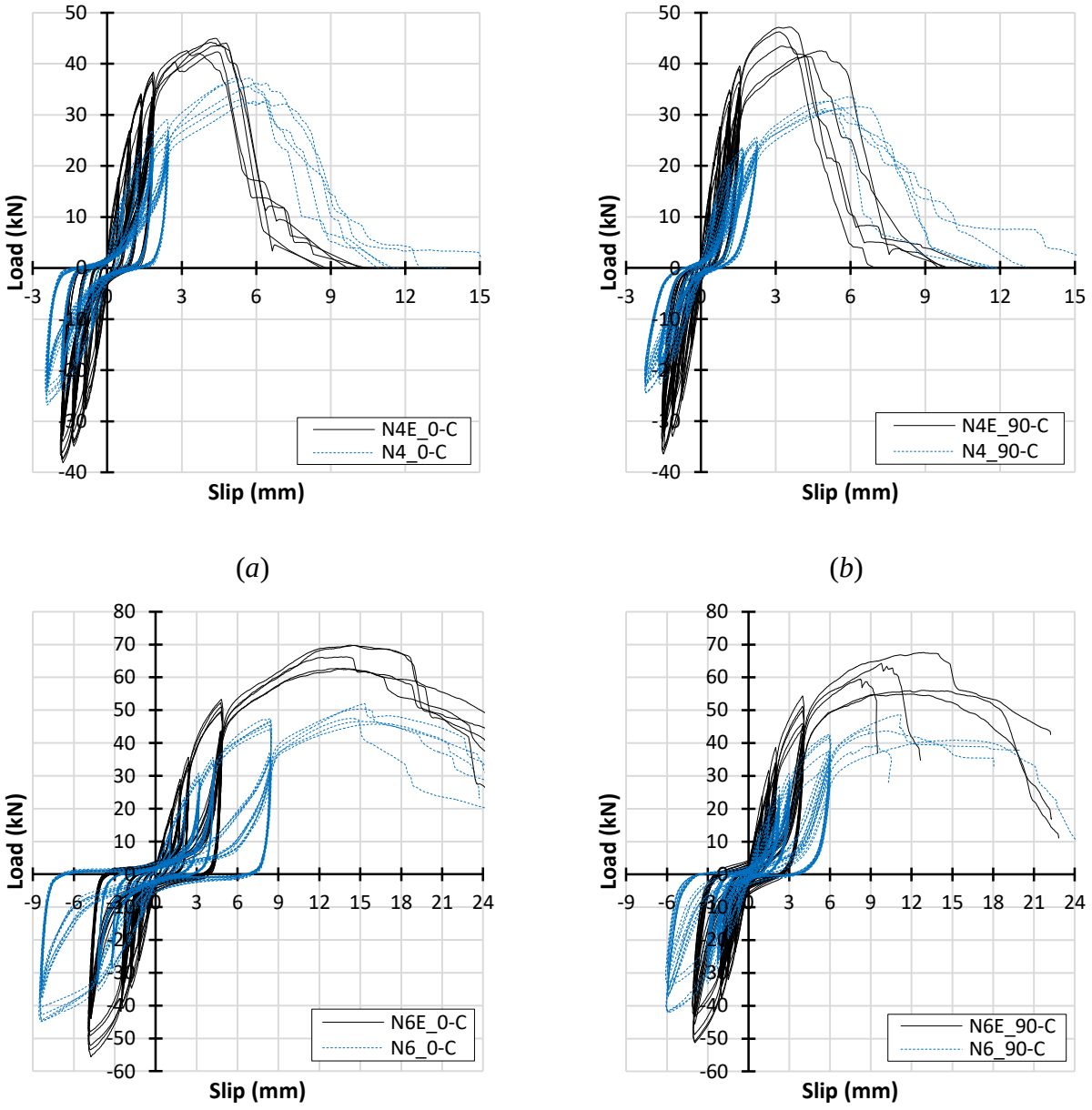

Figure 6. Experimental cyclic force-slip curves of unreinforced samples (dashed blue lines) superimposed to strengthened samples (continuous black lines).

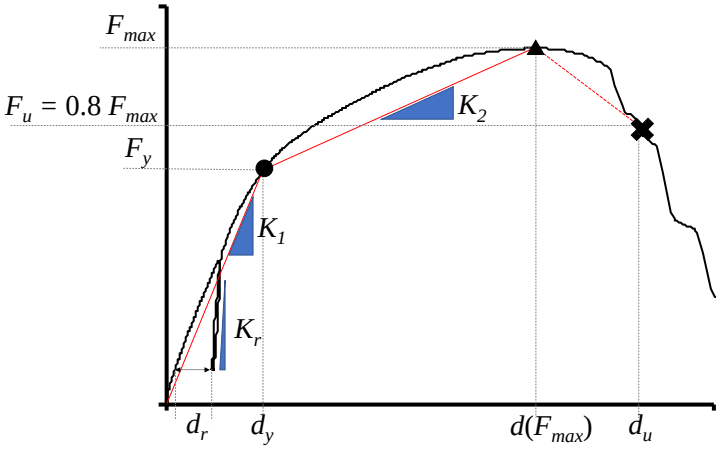

Figure 7. Scheme of the linearization of experimental force - slip curves: parameters assessed for monotonic and cyclic tests.

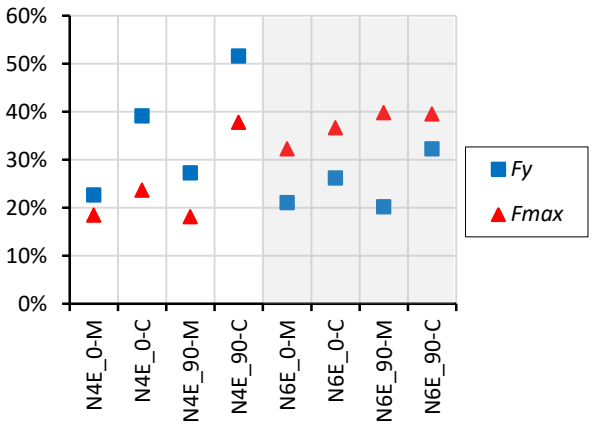

(*a*)

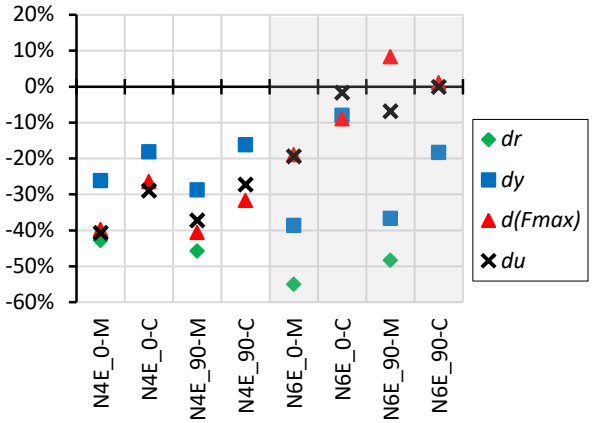

(*b*)

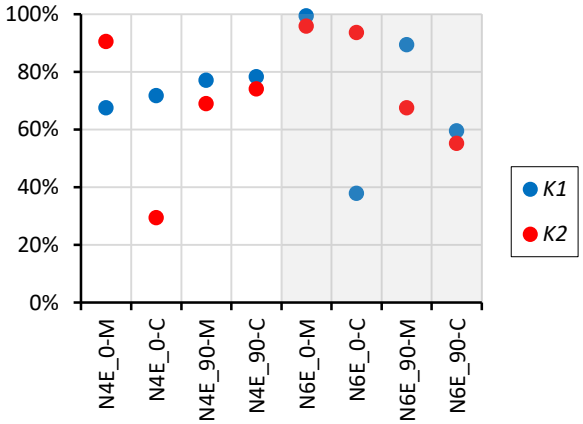

(*c*)

Figure 8. Parameters obtained from linearization: comparison, in terms of percentage difference, passing from unreinforced to strengthened samples; effect on: (*a*) forces; (*b*) displacements; (*c*) elastic and post-elastic stiffness.

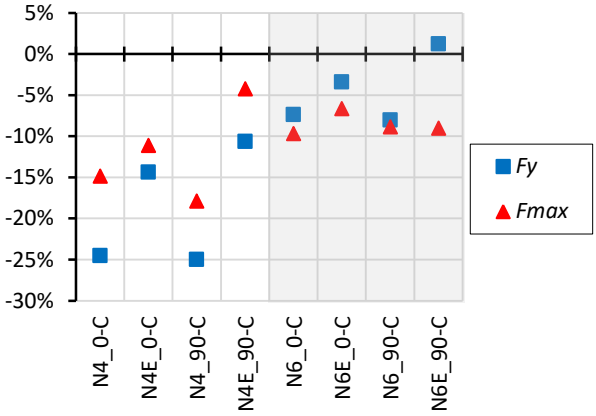

(*a*)

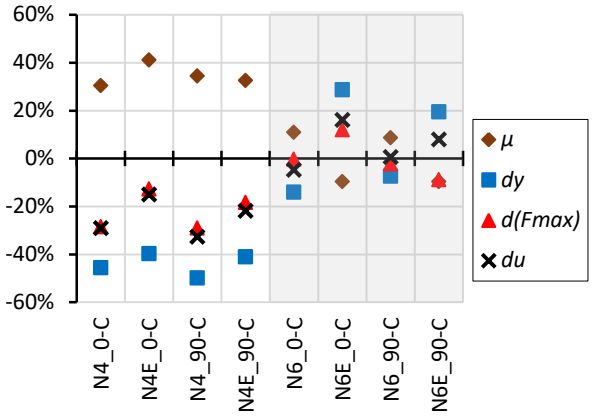

(*b*)

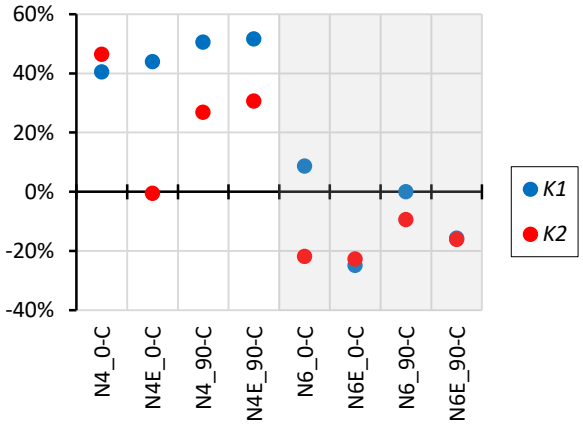

(*c*)

Figure 9. Parameters obtained from linearization: comparison, in terms of percentage difference, between cyclic and monotonic tests; effect on: (*a*) forces; (*b*) displacements and ductility; (*c*) elastic and post-elastic stiffness.